Front. Eng. Manag. 2024, 11(4): 620–632
https://doi.org/10.1007/s42524-023-0284-y

RESEARCH ARTICLE

Ying YANG, Kun GAO, Shaohua CUI, Yongjie XUE, Arsalan NAJAFI, Jelena ANDRIC

Data-driven rolling eco-speed optimization for autonomous vehicles

© The Author(s) 2024. This article is published with open access at link.springer.com and journal.hep.com.cn

Abstract In urban settings, fluctuating traffic conditions and closely spaced signalized intersections lead to frequent emergency acceleration, deceleration, and idling in vehicles. These maneuvers contribute to elevated energy use and emissions. Advances in vehicle-to-vehicle and vehicle-to-infrastructure communication technologies allow autonomous vehicles (AVs) to perceive signals over long distances and coordinate with other vehicles, thereby mitigating environmentally harmful maneuvers. This paper introduces a data-driven algorithm for rolling eco-speed optimization in AVs aimed at enhancing vehicle operation. The algorithm integrates a deep belief network with a back propagation neural network to formulate a traffic state perception mechanism for predicting feasible speed ranges. Fuel consumption data from the Argonne National Laboratory in the United States serves as the basis for establishing the quantitative correlation between the fuel consumption rate and speed. A spatiotemporal network is subsequently developed to achieve eco-speed optimization for AVs within the projected speed limits. The proposed algorithm results in a 12.2% reduction in energy consumption relative to standard driving practices, without a significant extension in travel time.

Keywords data-driven learning, speed optimization, autonomous vehicles, energy saving

Received Sep. 15, 2023; revised Oct. 19, 2023; accepted Oct. 22, 2023

Ying YANG
School of Management, Shanghai University, Shanghai 200444, China

Kun GAO, Shaohua CUI (✉), Arsalan NAJAFI
Department of Architecture and Civil Engineering, Chalmers University of Technology, Gothenburg 41296, Sweden
E-mail: shaohuac@chalmers.se

Yongjie XUE
School of Transportation Science and Engineering, Beihang University, Beijing 100191, China

Jelena ANDRIC
Department of Architecture and Civil Engineering, Chalmers University of Technology, Gothenburg 41296, Sweden; Volvo Group Trucks Technology, Gothenburg 40508, Sweden

This research was supported by VINNOVA (ICV-safe, 2019-03418), Energimyndigheten and JPI Urban Europe through e-MATS project (P2023-00029), and AI Center (CHAIR) at Chalmers University of Technology (CHAIR-CO-EAIVMS-2021-009).

Open access funding provided by Chalmers University of Technology.

1 Introduction

Countries worldwide are presently grappling with fuel shortages. The transportation industry's fuel consumption constitutes a significant share of the overall fuel utilization. In China, as of 2020, transportation accounted for 66% of total fuel consumption, with road transportation equipment, including both cars and heavy trucks, contributing 77% of the entire transportation equipment's fuel consumption (Jia et al., 2022). Reports indicate that nonenvironmentally friendly vehicle maneuvers, such as acceleration, deceleration, and idling, constitute 30%–40% of the total vehicle operating consumption. In urban settings, this proportion tends to be even higher (Kabir et al., 2023; Zhang et al., 2023). These nonenvironmentally friendly vehicle actions not only result in increased vehicle energy consumption but also trigger greater acceleration and deceleration among upstream vehicles, leading to what is commonly referred to as traffic waves (Cui et al., 2022a; Guo et al., 2023; Jafaripournimchahi et al., 2023). Such traffic jam waves can even emerge on highways devoid of intersections, as seen in phantom traffic jams (Goldmann and Sieg, 2020). Consequently, judicious eco-speed optimization can mitigate not only a vehicle's fuel consumption but also the substantial fuel consumption induced in upstream vehicles.

Advancements in vehicle-to-vehicle and vehicle-to-infrastructure communication technologies enable autonomous vehicles (AVs) to access signal phase and vehicle state information beyond their line of sight (Ali et al., 2021; Dong et al., 2022; Zhu et al., 2022). Numerous studies have demonstrated that information regarding the state of surrounding vehicles promotes traffic flow stability

based on methods such as Fourier Ansatz linear stability (Jiang et al., 2021; Yu et al., 2021; Cui et al., 2022a), Lyapunov stability (Larsson et al., 2021; Cui et al., 2022b; 2023), and others. However, these studies often overlook the influence of signal phase changes at intersections on traffic flow stability. The transition between red and green signal phases can readily trigger abrupt braking and acceleration among vehicles. The traffic flow stability established in prior research can be disrupted by signal phase changes, particularly in urban environments characterized by close-proximity signalized intersections. Thus, the optimization of vehicle trajectories to ensure smooth travel must account for both surrounding vehicle state information and intersection signal phases.

Certain studies have contemplated the influence of information about surrounding vehicles on the optimization of vehicle trajectories. Wu et al. (2011) devised an environmental perception system to anticipate forthcoming road conditions by utilizing feedback information from road environment perception. They applied the Lagrangian algorithm to optimize vehicle acceleration and deceleration, with the aim of minimizing fuel consumption. Wang et al. (2017), Almannaa et al. (2019), Yang et al. (2016; 2021), and Liu et al. (2023) introduced a microlevel eco-speed optimization strategy employing fleet concepts and heuristic algorithms to achieve energy efficiency and emissions reduction. Barth and Boriboonsomsin (2009) furnished drivers with real-time updates concerning fluctuating traffic conditions, including speed, density, and traffic status near their vehicles, along with dynamic recommendations. They observed that fuel consumption could be reduced by approximately 10%–20% without significantly extending travel time. Kamal et al. (2010) harnessed vehicle dynamics models and traffic flow models to predict the future state of the vehicle–road–traffic network. They estimated fuel consumption based on predicted future traffic conditions and subsequently generated optimal control inputs for eco-friendly driving. Chen et al. (2022) employed model predictive control to optimize vehicle ecological driving trajectories, accounting for the uncertainty associated with intersection queues and signal phases. Reza Amini et al. (2020) introduced a multirange speed prediction framework that accommodated varying levels of fidelity across different forecast time step ranges. This framework was integrated with model predictive control to optimize ecological vehicle trajectories.

Some studies examine the influence of both the current and future signal phases at intersections on vehicle trajectories. Asadi and Vahidi (2011) incorporated signal phase information at future time steps into an adaptive cruise control system to reduce vehicle idling time at intersections, subsequently curbing fuel consumption. Similarly, Shi et al. (2018) harnessed signal phase information at future time steps but aimed to maximize the likelihood of vehicles traversing multiple consecutive intersections while the signals were green. In the context of continuous intersections, several research endeavors have centered on devising optimal vehicle trajectories through various algorithms, including the A* algorithm (Hu et al., 2018), Dijkstra algorithm (de Nunzio et al., 2016; Wu et al., 2021), genetic algorithm (Luo et al., 2017; Li et al., 2018), Markov chain (Li and Gopalswamy, 2021), receding dynamic programming (Guo and Wang, 2019), pseudospectral method (Wu et al., 2023), and model predictive control (Liu et al., 2021; Pi et al., 2022). Liu et al. (2022) directly incorporated signal phase information from multiple intersections into a deep reinforcement learning network to train eco-driving trajectories for vehicles. Ma et al. (2021) introduced two dynamic programming algorithms designed to optimize the speed trajectory of fleets, ensuring that fleets can pass through consecutive signalized intersections without separation.

To our knowledge, only a limited number of studies have considered the joint influence of both traffic conditions and signal phases at intersections on the optimization of environmentally friendly vehicle trajectories. Munoz-Organero and Magana (2013) developed an ecological driving assistance system for detecting traffic signals. However, their approach relied on information from nearby vehicles and signal phases exclusively to optimize vehicle speeds as they approached intersections. Zhang et al. (2020) employed deep learning models to predict traffic flow and devised an efficient red light duration model based on traffic flow queuing dynamics. They proposed a constrained optimization model to adjust vehicle speeds, reducing computation time. Nevertheless, none of the aforementioned studies took into account the effect of traffic conditions in upstream lanes and signal phases at upstream intersections on speed trajectory optimization. Neglecting these factors can lead to excessively high optimal speeds, given their substantial influence on the feasible speed range for AVs. The presence of slow-moving AVs or delays resulting from red signal phases can lead to a significant number of AVs with minimal intervehicle gaps on the upstream road. When these slow-moving AVs exit or change lanes or when the red signal transitions to green, these closely spaced AVs may encounter traffic saturation or even oversaturation on the downstream segment. In accordance with traffic flow theory, this significantly narrows the feasible speed range for vehicles. Thus, the traffic status on the upstream segment and the signal phase at upstream intersections play pivotal roles in optimizing eco-friendly vehicle speeds. Furthermore, the optimized speed serves as a crucial input for predicting the feasible speed range, further enhancing the prediction accuracy.

This paper addresses the data-driven rolling eco-speed optimization challenge for AVs, focusing on the optimization of vehicle maneuvers. We introduce a short-term speed forecasting algorithm to provide a feasible speed range, and rolling AV eco-speed optimization is

conducted within this range. This paper makes significant contributions to related research in three key aspects: 1) We combine backpropagation (BP) neural networks and deep belief networks (DBNs) to real-time predict the short-term feasible speed range, considering traffic conditions in both upstream and downstream lanes and signal phases at upstream and downstream intersections; 2) We construct a space–time network of speed and propose a rolling eco-speed optimization algorithm for AVs at consecutive intersections based on the Dijkstra algorithm; and 3) We utilize data from the Argonne National Laboratory in the United States to precisely establish the quantitative relationship between fuel consumption rates and speed.

The subsequent sections of this paper are organized as follows. Section 2 provides an elaborate description of the data-driven rolling optimization problem. Section 3 combines BP and DBN to forecast the traffic state. Section 4 introduces a rolling eco-speed optimization algorithm grounded in the Dijkstra algorithm. Section 5 validates the aforementioned algorithms. And finally, Section 6 summarizes this paper and outlines potential avenues for future research.

2 Problem description

This paper focuses on optimizing the eco-speed of AVs as they traverse consecutive intersections, as depicted in Fig. 1. While factors such as phase cycle length, the overlap ratio of green phases, and speed limits at intersections and links have a significant effect on eco-speed optimization, it is crucial to recognize the pivotal role played by traffic conditions in this optimization process. For instance, consider the scenario where traffic flow exhibits small intervehicle gaps, a situation exacerbated by slow-moving traffic along the upstream links. Such a condition can potentially lead to congestion or even saturation of downstream links during the subsequent time step. Similarly, the presence of slow-moving traffic on downstream links can impede the entry of traffic from upstream links. As a result, vehicle speeds on the saturated links often fall considerably below the prescribed speed limits.

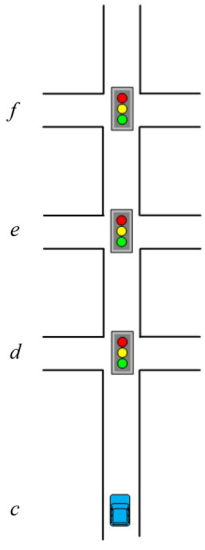

Fig. 1 Consecutive intersections.

To achieve a more practical eco-speed that aligns with the prevailing road operating conditions, this paper introduces a data-driven rolling eco-speed optimization algorithm. This algorithm leverages historical and real-time traffic state data to generate short-term forecasts of the feasible speed range for AVs, as depicted by the dotted lines in Fig. 2. Subsequently, the algorithm formulates real-time rolling eco-speed plans based on these prediction results, as indicated by the solid line in Fig. 2.

3 Traffic state prediction

The current road traffic conditions impose significant constraints on the operational speeds of AVs. Achieving precise optimization of the effective eco-speed for AVs navigating consecutive intersections necessitates a comprehensive consideration of the traffic state, particularly within the interconnected upstream and downstream links. Furthermore, the signal phases at both the intersection where the AV is approaching and the downstream intersection also influence the eco-speed planning for the AV. In cases where the AV cannot clear the downstream intersection through rapid acceleration during the current green phase, a judicious approach involves gradual acceleration to ensure arrival at the intersection in time for subsequent green phase activation. This strategy mitigates the adverse effects of rapid acceleration and idling, thus minimizing fuel consumption.

Therefore, before optimizing the AV eco-speed, this section makes a short-term prediction of the feasible speed range based on the traffic state of upstream and downstream links and the signal phases of upstream and

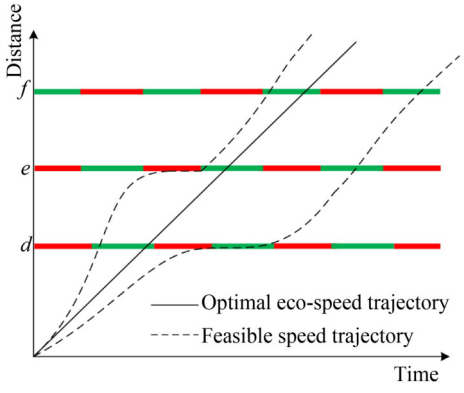

Fig. 2 Rolling eco-speed optimization.

downstream intersections. Let us take the continuous links in Fig. 1 as an example to explain the rolling prediction of the feasible speed range. When the AV, running on link (c, d), approaches intersection d, it predicts its feasible speed range for running on link (d, e) using the traffic state data of links (c, d) and (d, e) and the signal phases of intersections c and d. Subsequently, the AV optimizes its speed through intersection d according to the eco-speed optimization algorithm in Section 4. Finally, the AV optimizes its speed passing through link (d, e) based on the optimized speed passing through intersection d and the signal timing at intersection e. When the AV approaches intersection e, the above feasible speed range prediction and eco-speed optimization are repeated.

While traffic density and congestion index can effectively reflect the state of links, speed is a more readily measurable variable compared to them. Therefore, this paper selects the speed $v_{cd,t}$ on link (c, d) at time slot t as the state evaluation value of the link. Based on the preceding discussion, the input of the predictive model can be expressed as follows:

$$\hat{v}_{de,t} = f\left(v_{cd,t},\ v_{de,t-1},\ v_{ef,t+1},\ L_d,\ L_e\right), \tag{1}$$

where $\hat{v}_{de,t}$ is the predicted value of speed $v_{de,t}$ on link (d, e) at time step t. L_d and L_e represent the signal phase periods of intersections d and e, respectively.

DBN is an artificial neural network designed to emulate the cognitive reasoning process of the human brain. DBNs have found extensive applications across various domains, including image and speech processing. As a deep learning model, DBN exhibits remarkable predictive accuracy and effectiveness when dealing with nonlinear, nonstationary, and uncertain traffic flow data. When confronted with large volumes of raw data, DBN excels at extracting meaningful data characteristics, making it particularly well suited for addressing regression problems. A DBN is characterized as an arbitrary undirected graph probabilistic generative model. It consists of multiple layers of random neurons positioned between the input layer and the output layer. These neurons can be classified into explicit neurons, responsible for receiving input, and hidden neurons, also known as feature detectors, which are responsible for feature extraction. The connections among the upper layers of neurons in a DBN are undirected, forming a shared memory structure. In contrast, the connections among the lower-layer neurons are directed and represent data vectors, with the dimensionality of the data vector scaling with the number of neurons.

A DBN consists of a set of restricted Boltzmann machines (RBMs) (Fig. 3), which provide feature learning and feature extraction capabilities for DBNs. RBM consists of neurons (i.e., $\upsilon = [\upsilon_1, \upsilon_2, ..., \upsilon_i, ..., \upsilon_m]^{\mathrm{T}}$) in the display layer and neurons in the hidden layer (i.e., $h = [h_1, h_2, ..., h_j, ..., h_k]^{\mathrm{T}}$), where the neurons in the display layer are used to input training data, and the

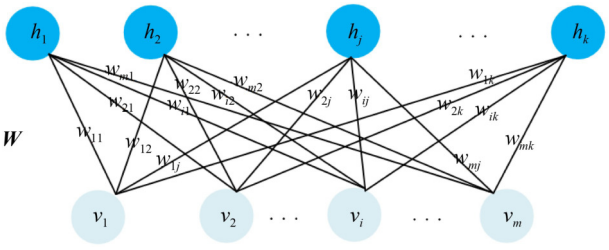

Fig. 3 Restricted Boltzmann machines.

neurons in the hidden layer are used for feature detection. The m-by-k-dimensional $W = \begin{bmatrix} w_{11} & ... & w_{1k} \\ ... & ... & ... \\ w_{m1} & ... & w_{mk} \end{bmatrix}$ is the weight matrix between the neurons in the display layer and the neurons in the hidden layer.

Typically, neurons in RBM are constrained to assume values of either 0 or 1, which imposes limitations on its applicability to practical problems. Given that traffic data are continuous, this paper introduces the Gauss-Bernoulli restricted Boltzmann machine (GBRBM), which is capable of handling continuous data. In this model, neurons in the visible layer follow a Gaussian distribution, while neurons in the hidden layer follow a Bernoulli distribution. The GBRBM is an energy-based model that utilizes neurons in the hidden layer to characterize the probability distribution of neurons in the visible layer.

The joint energy function can be obtained by introducing Gaussian noise with standard deviation $\sigma = [\sigma_1, \sigma_2, ..., \sigma_i, ..., \sigma_m]^{\mathrm{T}}$ in neurons $\upsilon = [\upsilon_1, \upsilon_2, ..., \upsilon_i, ..., \upsilon_m]^{\mathrm{T}}$ in the display layer as follows:

$$E(\upsilon, h) = -\sum_{i=1}^{m} \frac{(\upsilon_i - a_i)^2}{2\sigma_i^2} - b^{\mathrm{T}}h - h^{\mathrm{T}}W\frac{\upsilon}{\sigma}, \tag{2}$$

where $a = [a_1, a_2, ..., a_i, ..., a_m]^{\mathrm{T}}$ and $b = [b_1, b_2, ..., b_j, ..., b_k]^{\mathrm{T}}$ represent the bias vectors of neurons in the display layer and neurons in the hidden layer, respectively. Since the neurons in the visible and hidden layers are connected independently, they are independent of each other. We can obtain the following conditional probabilities:

$$P(h_j = 1|\upsilon) = \mathrm{sigmoid}\left(b_j + \sum_{i=1}^{m} \frac{\upsilon_i}{\sigma_i} w_{ij}\right), \tag{3}$$

$$P(\upsilon_i|h) = N\left(a_i + \sigma_i \sum_{j=1}^{k} w_{ij}h_j,\ \sigma_i^2\right), \tag{4}$$

where the function $\mathrm{sigmoid}(\cdot)$ is defined as $\mathrm{sigmoid}(\cdot) = \frac{1}{1+\exp(\cdot)}$, and $N(\mu, \sigma^2)$ represents a Gaussian distribution with mean μ and variance σ^2. It is difficult to directly estimate the structural parameters $a = [a_1, a_2, ..., a_i, ..., a_m]^{\mathrm{T}}$, $b = [b_1, b_2, ..., b_j, ..., b_k]^{\mathrm{T}}$, and $W =$

$\begin{bmatrix} w_{11} & \cdots & w_{1k} \\ \cdots & \cdots & \cdots \\ w_{m1} & \cdots & w_{mk} \end{bmatrix}$ of the GBRBM by minimizing the negative log-likelihood. In this paper, the random approximation method of Gibson sampling with a limited number of iterations (also known as the contrastive divergence algorithm) is used to update the structural parameters as follows:

$$\Gamma = \log \Pi_m P(\upsilon_m), \tag{5}$$

$$\Delta w_{ij} = \varepsilon \frac{\partial \Gamma}{\partial w_{ij}} = \varepsilon \left(\left\langle \frac{\upsilon_i h_j}{\sigma_i^2} \right\rangle_d - \left\langle \frac{\upsilon_i h_j}{\sigma_i^2} \right\rangle_m \right), \tag{6}$$

$$\Delta a_i = \varepsilon \frac{\partial \Gamma}{\partial a_i} = \varepsilon \left(\left\langle \frac{\upsilon_i}{\sigma_i^2} \right\rangle_d - \left\langle \frac{\upsilon_i}{\sigma_i^2} \right\rangle_m \right), \tag{7}$$

$$\Delta b_j = \varepsilon \frac{\partial \Gamma}{\partial b_j} = \varepsilon \left(\left\langle \frac{h_j}{\sigma_i^2} \right\rangle_d - \left\langle \frac{h_j}{\sigma_i^2} \right\rangle_m \right), \tag{8}$$

where ε is the learning rate, and $\langle \cdot \rangle_d$ and $\langle \cdot \rangle_m$ represent the expected values of the training data and the model, respectively.

In the DBN model, data features are extracted from observed data using the hidden layer of a GBRBM. These data features are then utilized as inputs for another GBRBM, resulting in a multilayer structure created by stacking GBRBMs cyclically. It is important to note that the GBRBM is inherently designed for unsupervised learning. To transform it into a tool for supervised learning, it must be integrated with an additional supervised learning algorithm, such as the BP neural network. In this paper, the final output generated by the multilayer GBRBMs serves as input for the BP neural network, with the output of the BP neural network representing the prediction results. The combined algorithm framework that incorporates the multilayer GBRBMs and BP is depicted in Fig. 4.

4 Eco-speed optimization

AVs navigating urban roads frequently traverse multiple intersections and links. In a predefined route, each link presents distinct feasible speed ranges, and the corresponding methods for traversing intersections, including acceleration, deceleration, and maintaining a constant speed, vary. As a result, AVs have the flexibility to complete journeys using various combinations of speeds. In this paper, we discretize the speed and establish a coordinate system that employs time and space (position) as the horizontal and vertical axes, as illustrated in Fig. 5. The Dijkstra algorithm represents a classical shortest path algorithm, focusing on the origin node and systematically advancing through successive layers of nodes until reaching the endpoint. By utilizing the spatial–temporal network structure depicted in Fig. 5 and considering the vehicle energy consumption weights associated with the connecting links of spatial–temporal nodes, we apply the Dijkstra algorithm to determine the path with the lowest vehicle energy consumption.

When AVs are distant from intersections, optimizing their eco-speed only requires consideration of the speed limit on links and the traffic state of those links. The traffic state of links can be quantified using the feasible speed range of AVs predicted in the previous section. For simplicity, we refer to the upper limit of vehicle speed determined by the speed limit on links and traffic state as the speed limit V_L. This paper utilizes open-source data provided by Argonne National Laboratory in the United States to establish a quantified relationship between fuel consumption and the speed of AVs. Figure 6 illustrates the relationship between fuel consumption and vehicle speed. As observed in the figure, the relationship between fuel consumption and speed follows a pattern where fuel consumption initially increases, then decreases, and eventually increases again with increasing speed. Prior to reaching the critical speed value, the relationship between fuel consumption and speed is nearly symmetrical around

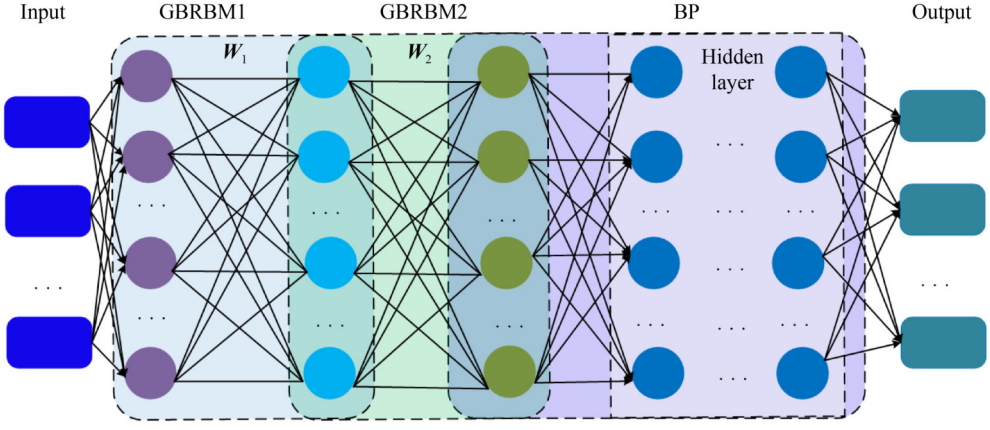

Fig. 4 Combined algorithm framework of multi-layer GBRBMs and BP.

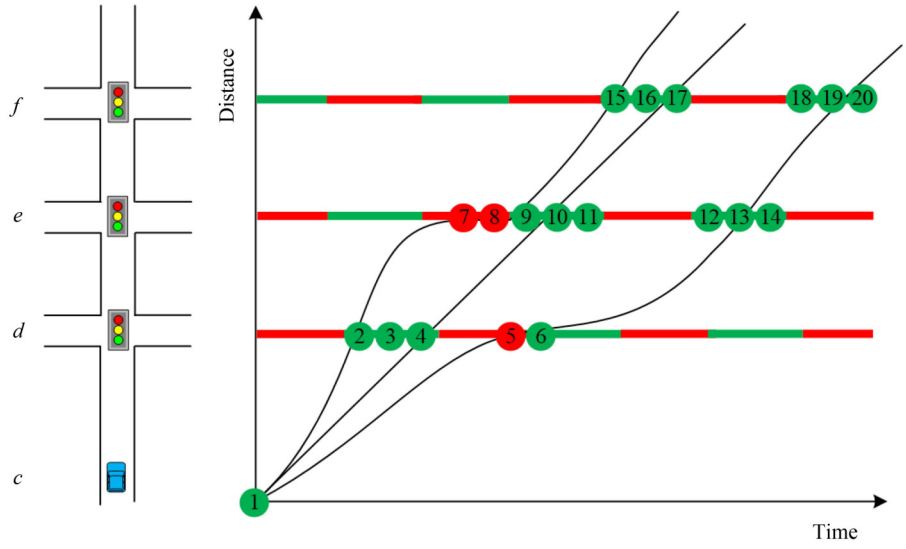

Fig. 5 Space–time network.

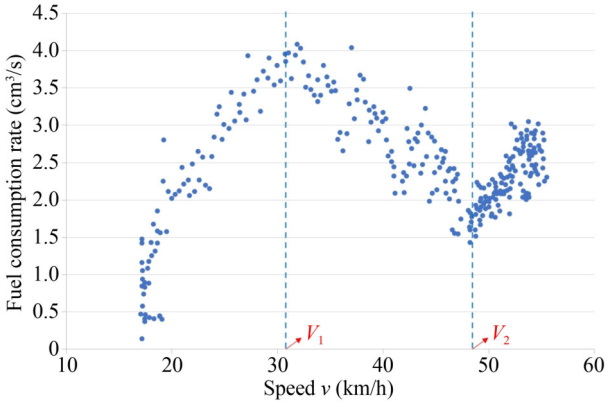

Fig. 6 Fuel consumption rate versus speed (source: Argonne National Laboratory (2023)).

this point. Before the speed reaches the critical value V_2, the relationship between fuel consumption and speed is almost symmetrical about $v = V_1$. Therefore, when the limit speed V_L is less than V_2, the optimal eco-speed is V_L. This is because when the vehicle speed is V_L, it can not only reduce energy consumption but also improve traffic efficiency. When the speed limit V_L is greater than V_2, the optimal eco-speed is V_2. According to the above analysis, when AVs are far from intersections, the optimal speed V_{opt} satisfies $V_{opt} = \min\{V_L, V_2\}$.

It can be seen from Fig. 6 that the idling of AVs will also cause high energy consumption. Therefore, when AVs approach intersections, their eco-speed optimization needs to consider the signal phase of intersections to avoid idling. Let $g_{c,l}$ be the time step at which the l-th green light phase at intersection c starts. Let $r_{c,l}$ be the time step at which the red light phase starts after the l-th green light phase at intersection c. If the time t when the AV arrives at intersection c satisfies $t \in (g_{c,l}, r_{c,l})$, the AV can pass through intersection c directly. If the time t when the AV arrives at intersection c satisfies $t \in (r_{c,l}, g_{c,l+1})$, the AV cannot pass through intersection c, so it can only wait at idle speed at the intersection. s represents the distance from the AV to the nearest downstream intersection. Let F_{idle} be the fuel consumption rate when AVs are waiting at idle speed at intersections. Let t_{idle} be the time step when AVs are idling at intersections.

According to the signal phase when AVs arrive at intersections, this paper divides the eco-speed optimization of the AVs passing intersections into the following two cases.

Case I: If the AV arrives at the intersection at speed V_2, the signal light is green, i.e., the time $t = s/V_2$ for the AV to reach the intersection at speed V_2 satisfies $t \in (g_{c,l}, r_{c,l})$.

(1) If $V_2 \leqslant V_L$, then the AV passes through the intersection at a constant speed V_2.

(2) If $V_2 > V_L$, then the AV can only reach the intersection at speed V_L at the fastest. We discuss this in the following two situations:

- If the traffic light is green when the AV arrives at the intersection at speed V_L (i.e., $(s/V_L) \in (g_{c,l}, r_{c,l})$), then the AV passes through the intersection at a constant speed V_L;
- If the signal light is red when the AV arrives at the intersection, the AV can choose to wait at the intersection by idling or perform speed optimization to ensure that it passes the intersection just when the red light ends. In the case of idling, the fuel consumption of the AV is $F_c(V_L)(s/V_L) + F_{idle}(g_{c,l+1} - s/V_L)$, where $F_c(\cdot)$ is the relationship function between the speed and fuel consumption rate. In the case that the AV passes the intersection just at the end of the red light, the fuel consumption of the AV is $F_c(s/g_{c,l+1})g_{c,l+1}$. If the fuel consumption of the former is less than that of the latter, the AV waits at the idling speed at the intersection. If the fuel consumption of the former is greater than that of the latter, the AV passes the

intersection at the end of the red light at speed $s/g_{c,l+1}$.

Case II: If the AV arrives at the intersection at speed V_2, the signal light is red, i.e., the time $t = s/V_2$ for the AV to reach the intersection at speed V_2 satisfies $t \in (r_{c,l},\ g_{c,l+1})$.

(1) If $V_L \geqslant s/r_{c,l} \geqslant V_2$, the AV can reach the intersection before the red light ends while meeting the speed limit V_L. Therefore, the AV can choose the following three ways to pass through the intersection: Accelerating to pass the intersection before the end of the green light; driving at a constant speed V_2 and waiting at the intersection at an idle speed; and decelerating to ensure that the AV passes the intersection when the red light ends. The fuel consumption in the above three intersection passing ways is $F_c(s/r_{c,l})r_{c,l}$, $F_c(V_2)(s/V_2)+F_{\text{idle}}(g_{c,l+1}-s/V_2)$ and $F_c(s/g_{c,l+1})g_{c,l+1}$, respectively. The AV chooses the way with the least fuel consumption to pass through the intersection.

(2) If $s/r_{c,l} \geqslant V_L \geqslant V_2$, the AV cannot reach the intersection before the red light ends. There are two ways for the AV to pass through the intersection: driving at a constant speed V_2 and waiting at an idling speed after reaching the intersection and decelerating so that the AV arrives at the intersection after the red light ends. The fuel consumption of the above two intersection passing ways is $F_c(V_2)(s/V_2)+F_{\text{idle}}(g_{c,l+1}-s/V_2)$ and $F_c(s/g_{c,l+1})g_{c,l+1}$, respectively. AVs choose the way with the least fuel consumption from the above two ways to pass through the intersection.

(3) If $V_2 \geqslant V_L \geqslant s/g_{c,l+1}$, the AV cannot travel at an eco-speed V_2 below the speed limit V_L and can only reach the intersection when the next green light starts. Therefore, there are two ways for an AV to pass through the intersection: Arriving at the intersection at a limited speed V_L and waiting at idle speed and passing through the intersection at a constant speed when the next green light starts. The fuel consumption of the two intersection passing ways is $F_c(V_L)(s/V_L)+F_{\text{idle}}(g_{c,l+1}-s/V_L)$ and $F_c(s/g_{c,l+1})g_{c,l+1}$, respectively. AVs can choose the way with the least fuel consumption to pass through the intersection.

(4) If $s/g_{c,l+1} \geqslant V_L$, the AV can only pass the intersection at the current speed limit V_L or slow down so that it can reach the intersection at the beginning of the next green phase. We further analyze the above two ways as follows:

- If the intersection is in the green phase when the AV travels to the intersection at speed V_L, the optimal eco-speed of the AV passing through the intersection is constant speed V_L.
- If the intersection is a red phase when the AV travels to the intersection at speed V_L, then the two ways for the AV to pass through the intersection are driving to the intersection at speed V_L and then idling to pass and just arriving at the intersection at the beginning of the next green phase. The fuel consumption of the above two ways of passing through the intersection are $F_c(V_L)(s/V_L)+F_{\text{idle}}(g_{c,l+1}-s/V_L)$ and $F_c(s/g_{c,l+1})g_{c,l+1}$, respectively.

During the above eco-speed optimization process, AVs may need to accelerate or decelerate to reach the eco-speed. According to Xia et al. (2013), when the speed of AVs is changed based on the sinusoidal trigonometric function, the acceleration rate and deceleration rate of AVs are moderate, which can ensure driving comfort and ecological fuel consumption. The vehicle speed change equation based on the cos function is as follows:

$$v=\begin{cases} V_h - V_d\cos(mt) & t\in\left[0,\ \dfrac{\pi}{2m}\right] \\ V_h - \dfrac{m}{n}V_d\cos\left(n\left(t-\dfrac{\pi}{2m}+\dfrac{\pi}{2n}\right)\right) & t\in\left[\dfrac{\pi}{2m},\ \left(\dfrac{\pi}{2m}+\dfrac{\pi}{2n}\right)\right], \\ V_h - \dfrac{m}{n}V_d & t\in\left[\left(\dfrac{\pi}{2m}+\dfrac{\pi}{2n}\right),\ \dfrac{s}{V_h}\right] \end{cases} \tag{9}$$

where V_h is the current speed, V_d is the difference between the initial speed and the desired speed, and m and n are parameters. To obtain the optimal acceleration curve, it is necessary to determine the values of parameters m and n. Xia et al. (2013) assumed that the time for the AV to adjust speed is T, and the value range of parameter m considering fuel consumption economy and driver comfort is $3.08/T \leqslant m \leqslant 2\pi/T$. The value range of n is determined by the following equation:

$$n^2 - mn\left(Tm-\frac{\pi}{2}\right)-m^2\left(1-\frac{\pi}{2}\right)=0. \tag{10}$$

5 Numerical simulations

This section conducts numerical simulations to validate the efficacy of the algorithms presented in this paper. Section 5.1 provides an overview of the simulation setup, while Section 5.2 conducts comparative simulations to validate the performance of the rolling forecast algorithm proposed in this paper. Furthermore, Section 5.3 evaluates the effectiveness of the eco-speed optimization algorithm.

5.1 Simulation setting

The numerical simulations in this study are conducted using Hutai Road in Shanghai, China, as illustrated in Fig. 7. Hutai Road has a total length of 5.33 km, starting from Zhijiang Road and ending at Jiangchang West Road. It is divided into five distinct links, each with specified lengths, red light intervals, and green light intervals, as outlined in Table 1. In Shanghai, every taxi is equipped with a vehicle-mounted GPS receiver that transmits data every ten seconds, including latitude, longitude, and reception timestamps, among other information. The

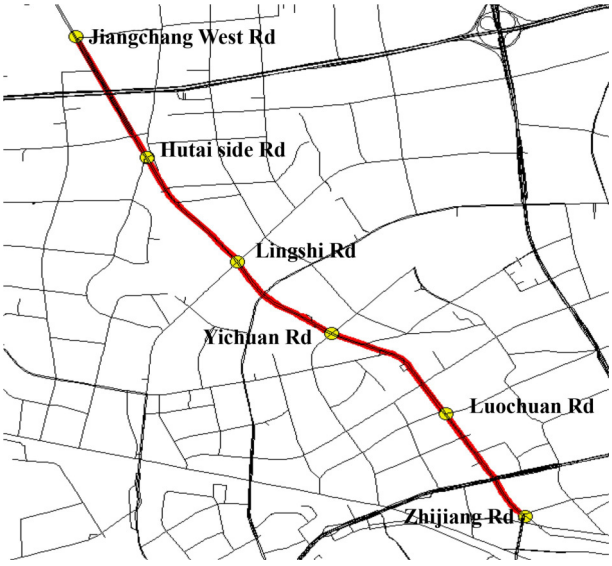

Fig. 7 Huitai Road in Shanghai, China.

Table 1 Link length, red light interval and green light interval at intersections

Link No.	Link start and end	Link length (m)	Green light interval (s)	Red light interval (s)
Link 1	Zhijiang Road–Luochuan Road	1042	20	30
Link 2	Luochuan Road–Yichuan Road	1089	30	40
Link 3	Yichuan Road–Lingshi Road	927	60	70
Link 4	Lingshi Road–Hutai side Road	1118	40	60
Link 5	Hutai side Road–Jiangchang West Road	1152	–	–

proportion of information that cannot be transmitted due to delays or communication failures is less than 10%. For this study, we collected GPS feedback data from all taxis traveling along the selected road during March 2016.

It is widely acknowledged that the vehicle fuel consumption rate is a function of vehicle speed. However, the speed of taxis is not explicitly provided by the vehicle-mounted GPS receiver. Therefore, we calculate the speeds of the taxis by leveraging the latitude and longitude information, along with the reception timestamps, after performing map matching. The following equation is employed to convert latitude and longitude information into the distance between two points, denoted as points A and B:

$$d = R \times \frac{\pi}{180} \times \mathrm{Arccos}(\sin(Lat\mathrm{A}) \times \sin(Lat\mathrm{B}) + \cos(Lat\mathrm{A}) \times \cos(Lat\mathrm{B}) \times \cos(Lon\mathrm{A} - Lon\mathrm{B})), \tag{11}$$

where d is the spherical distance between two points A and B, R is the radius of the earth, LonA and LonB are the longitudes of points A and B, respectively, and LatA and LatB are the latitudes of points A and B, respectively.

The accuracy of the GPS data is approximately 90%. Inaccurate data may result from equipment errors and transmission issues. Consequently, it becomes necessary to filter out calculated abnormal speeds. In conjunction with the speed limits on roads in Shanghai, this paper excludes data points where the speed is higher than 80 km/h.

From the data, it becomes evident that there is a considerable variance in the speeds of taxis at the same time step within the same link. Utilizing all the data as input for the DBN prediction algorithm in Section 3 may not effectively capture the traffic state of the link traversed by AVs. Consequently, this paper divides the historical data into two separate datasets based on their numerical values. These sets are then employed as input for the speed prediction algorithm, allowing the prediction algorithm to provide a feasible speed range.

5.2 Prediction numerical simulation

In this paper, 80% of the collected data serve as the training set, while the remaining 20% are allocated for the test set. The parameters in the DBN prediction model, including the number of layers (T), the number of visible layer units (m), the number of hidden layer units (k), the number of iterations (N), and the learning rate (ε), need to be trained. The ranges of these parameters are preset as $T \in [1, 4]$, $m \in [150, 200]$, $k \in [150, 200]$, $N \in [100, 500]$, and $\varepsilon \in [0.0005, 0.005]$ in this paper. After cross-validation of the training set data, the values of these parameters are finally determined to be $T = 2$, $m = 200$, $k = 200$, $N = 500$, and $\varepsilon = 0.005$.

This section uses the mean absolute percentage error (MAPE), mean absolute error (MAE) and root mean square error (RMSE) to evaluate the deviation between the predicted value and the actual observed value and to evaluate the accuracy of the predictive model. The calculation equation of each method is as follows:

$$\mathrm{MAPE} = \frac{1}{\eta}\sum_{t=1}^{\eta}\frac{\left|\hat{v}_{cd,t} - v_{cd,t}\right|}{v_{cd,t}} \times 100\%, \tag{12}$$

$$\mathrm{MAE} = \frac{1}{\eta}\sum_{t=1}^{\eta}\left|\hat{v}_{cd,t} - v_{cd,t}\right|, \tag{13}$$

$$\mathrm{RMSE} = \sqrt{\frac{1}{\eta - 1}\sum_{t=1}^{\eta}(\hat{v}_{cd,t} - v_{cd,t})^2}, \tag{14}$$

where η is the prediction time step.

The prediction model described in Eq. (1) incorporates a total of five input variables. To investigate the potential presence of redundant variables, we devised six sets of comparative models. Table 2 presents the results for these six groups of models, each with different input configurations, along with their respective MAPE results.

Table 2 Comparative models and MAPE values

Model	Input variables					MAPE
	$v_{cd,t}$	$v_{de,t-1}$	$v_{ef,t+1}$	L_d	L_e	
1		√	√	√	√	11.02%
2	√		√	√	√	12.89%
3	√	√		√	√	10.68%
4	√	√	√		√	10.28%
5	√	√	√	√		12.23%
6	√	√	√	√	√	9.31%

Upon comparing models 1, 2, and 3, it becomes evident that historical traffic state data from the current link exerts a more significant effect on prediction accuracy compared to data from the downstream link. This phenomenon can be attributed to the influence of vehicles from the upstream link in the previous time step entering the current link, thus significantly affecting vehicle speeds.

Similarly, when contrasting models 4 and 5, it becomes apparent that the signal phase of the downstream intersection has a more substantial effect on the prediction accuracy than the signal phase of the current intersection. This discrepancy arises from the signal phase of the downstream intersection, causing traffic flow on the current link to pause and await the signal change, thereby significantly impacting prediction accuracy.

Last, when comparing models 1 through 6, it becomes evident that model 6 yields the lowest MAPE value. Consequently, we adopt the influencing factors present in model 6 as the input variables for our DBN prediction model.

To assess the effectiveness of the proposed prediction algorithm, this paper employs support vector machines (SVMs), random forests (RFs), BP neural networks, and *K*-nearest neighbors (KNNs) as comparison algorithms. Figure 8 compares the performance of the five prediction models in terms of MAE, MAPE, and RMSE.

As shown in the figure, SVM, RF, and BP outperform KNN significantly. This improvement can be attributed to feature simplification in RF, which helps avoid overfitting issues. BP demonstrates a notable advantage in predicting data with substantial fluctuations. From the perspective of structural risk minimization, SVM analyzes various aspects of the learning process, including consistency, convergence speed, and more, resulting in its strong performance.

Among the five models, the DBN model achieves the highest prediction accuracy. To further substantiate the superior performance of the DBN model, a comparison is made between actual and predicted values across all five models, as illustrated in Fig. 9. The graphical representation clearly indicates that the DBN model exhibits the smallest deviation between actual and predicted values, resulting in a clustering of predicted points near the fitting line. This observation underscores the enhanced prediction accuracy achieved by the DBN model proposed in this study. In contrast, the actual values under the remaining four models deviate significantly from their corresponding predicted values, leading to a dispersed arrangement of predicted points. This discrepancy underscores the comparatively inferior prediction performance of these four algorithms when compared to the DBN model. These test results unequivocally affirm the DBN model's prowess in addressing short-term traffic flow forecasting, thereby meeting the precision criteria stipulated in this study. Consequently, the DBN model emerges as a valuable tool for providing the feasible speed range necessary for eco-speed optimization.

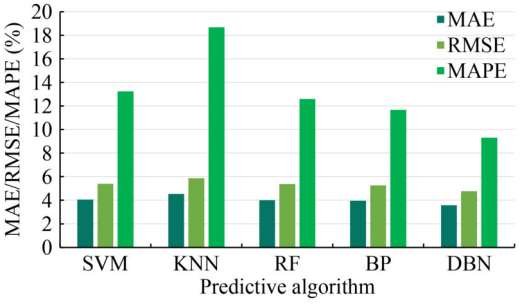

Fig. 8 MAE, MAPE and RMSE under different predictive algorithms.

To assess the influence of vehicle data arriving at intersections during different signal phases on the prediction results, the data are segregated into two sets: One comprising vehicles arriving at intersections during the red light period and the other during the green light period. These two new datasets are used as inputs separately, and the predicted results are displayed in Fig. 10.

From the figure, it is evident that the prediction accuracy varies between vehicle arrivals at intersections during different signal phases. This observation underscores the effect of the signal phase on the prediction process, validating the rationale for DBN to consider the signal phase as input for the prediction model. Additionally, the data of vehicles arriving at intersections during the green phase positively influence the model more than the data from the red phase, resulting in higher prediction accuracy for the model.

5.3 Eco-speed optimization

The prediction results regarding the feasible speed intervals for each link are presented in Table 3. This paper does not account for errors in eco-speed optimization stemming from prediction inaccuracies.

Figure 11 illustrates vehicle trajectories under three scenarios: eco-speed optimization considering traffic state (ES-TS), eco-speed optimization without considering traffic state (ES-WTS), and normal driving (ND). In the figure, the horizontal axis represents travel time, and the

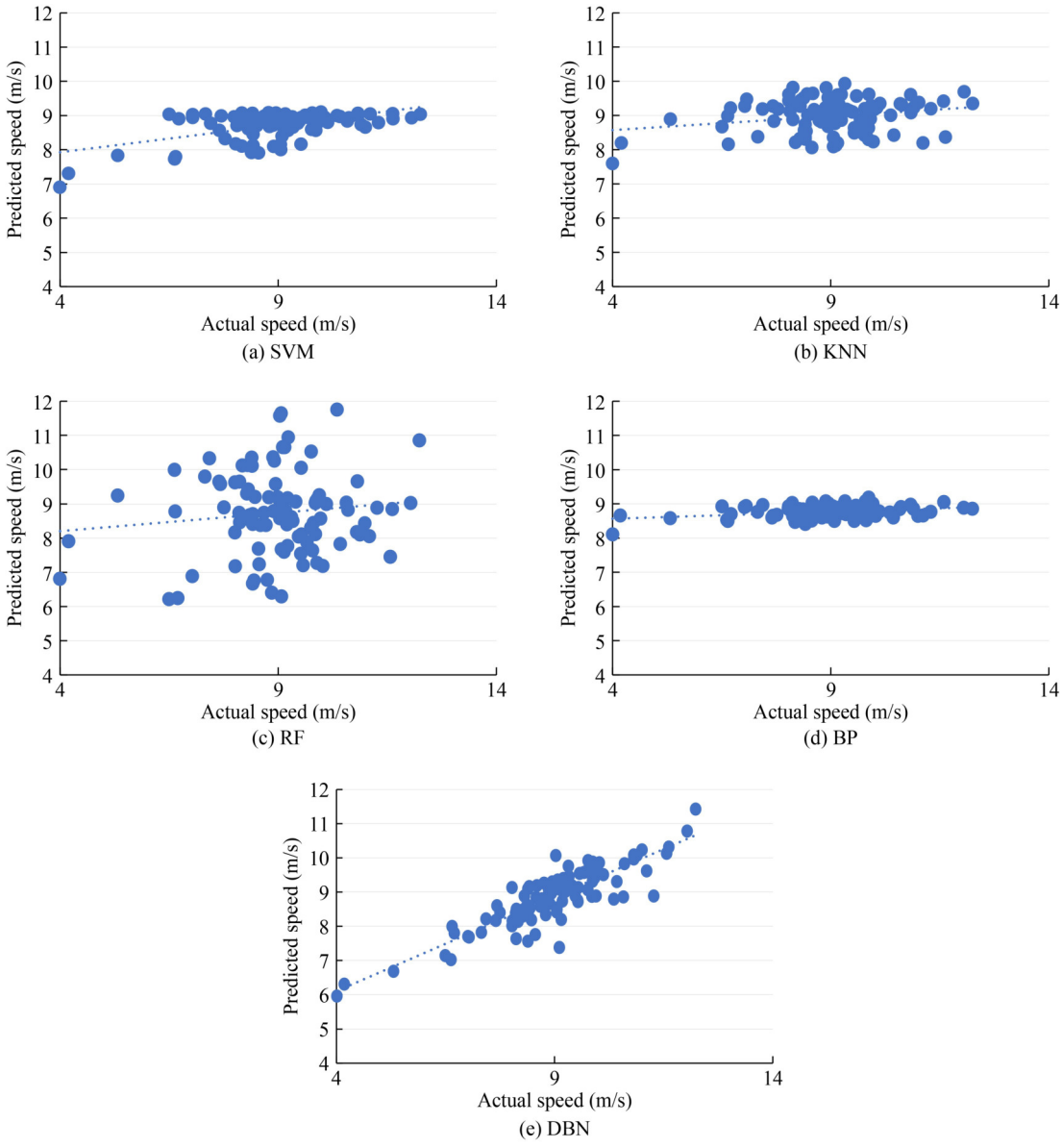

Fig. 9 Actual speed versus predicted speed.

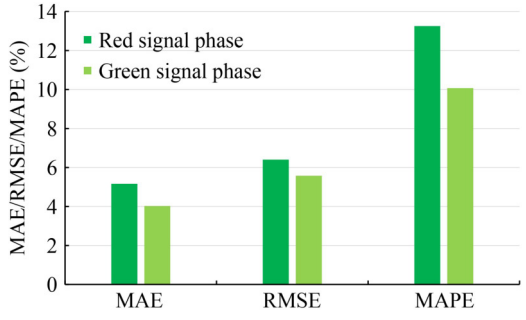

Fig. 10 MAE, MAPE and RMSE under different signal phases.

vertical axis represents distance traveled. The scale points on the vertical axis denote intersections. The red horizontal line signifies that the intersection is in the red phase, indicating that AVs are not allowed to pass. The time period between the red horizontal lines represents the green phase during which AVs can pass.

Table 3 The predicted feasible speed intervals

Link No.	Feasible speed intervals (m/s)
Link 1	11–16
Link 2	14–17
Link 3	8–11
Link 4	11–14
Link 5	20–22.2

The simulation results clearly demonstrate the advantages of eco-speed optimization considering the traffic state. For example, on the first link, the predicted feasible speed range is 11 to 16 m/s. Under ND, the AV on this

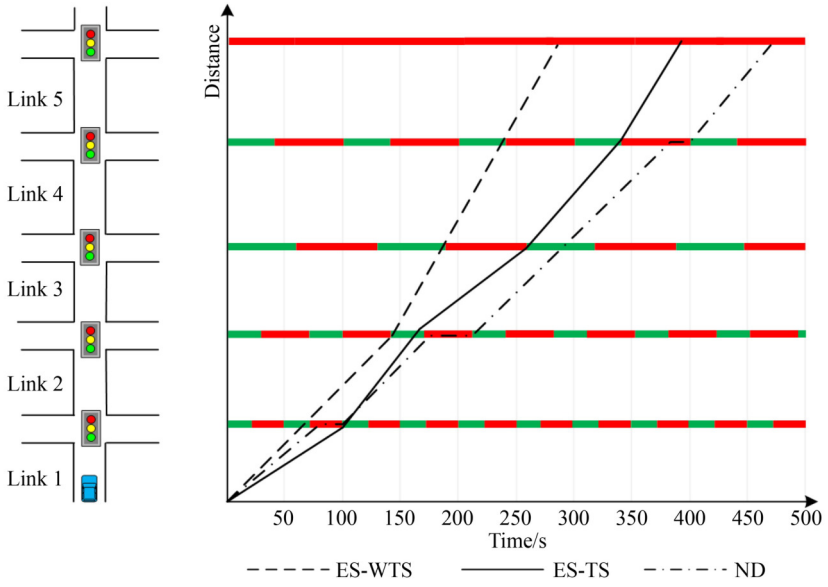

Fig. 11 Spatio–temporal trajectories of positions under different optimization algorithms.

link travels at maximum speed. However, at this time, the signal phase at the first intersection is red, necessitating the AV to wait at an idle speed. It is worth noting that fuel consumption at idle speeds cannot be underestimated. Therefore, with ES-TS, the AV travels at a speed that allows it to pass the first intersection just as the red light ends, eliminating the need to wait at an idle speed at the first intersection.

Similarly, on the second link with a predicted feasible speed range of 14 to 17 m/s, an AV traveling at this speed under ND cannot reach the second intersection before the green phase ends. This implies that the AV would have to wait at an idle speed at the second intersection. However, an AV under ES-TS starts with a certain initial speed when passing the first intersection, allowing it to arrive and pass the second intersection before the red light phase begins.

On the third link, with a predicted feasible speed range of 8 to 11 m/s, an AV traveling at this speed under ND can pass through the third intersection while the light is green. However, the AV speed optimized by ES-TS cannot pass the third intersection before the green light ends. Therefore, under ES-TS, AVs choose to reduce their speed and pass the third intersection just when the red light phase ends.

The predicted feasible speed range for the fourth link is 11 to 14 m/s. ES-TS determines that the AV at this speed can clear the fourth intersection before the next red light. Therefore, under this speed optimization, the AV chooses to accelerate and pass the intersection. Under ND, the AV can only wait at an idle speed when it reaches the fourth intersection.

On the fifth link, with a predicted feasible speed range of 20 to 22.2 m/s, the AV can travel at a relatively high speed. However, the theoretical eco-speed for the AV is 21 m/s. Therefore, under ES-TS, the AV runs at the theoretical eco-speed. Under ND, the AV travels to the end at a speed greater than 21 m/s.

Comparing ES-TS with ES-WTS reveals that the speed profile derived from the latter contradicts actual traffic conditions. ES-WTS results in speeds exceeding the feasible speed range, primarily to enable the AV to navigate the first intersection quickly. However, during the traversal of the third, fourth, and fifth links, the AV adheres solely to an eco-speed under the constraint of the road speed limit, without considering the prevailing traffic flow conditions.

The speed profiles for all three driving strategies depict the AV's characteristic acceleration and deceleration behavior at intersections, aligning with the real-world driving dynamics of AVs. Notably, under the ND strategy, the AV frequently undergoes sharp acceleration and deceleration, which is unfavorable for minimizing fuel consumption. In contrast, the vehicle speed profile under ES-TS maintains a more environmentally friendly speed and exhibits relative stability.

Table 4 presents the results of fuel consumption and travel time under the three driving strategies. It is evident from Table 4 that the eco-speed optimization algorithm considering traffic states yields a notable fuel-saving effect, achieving a fuel-saving efficiency of up to 12.2% when compared to the ND strategy. Furthermore, travel efficiency is maintained in terms of travel time, ensuring a positive travel experience for passengers.

On the other hand, the eco-speed optimization algorithm that does not consider traffic states reduces travel time but lacks practical significance. This is primarily because it does not account for the feasibility of speed. Additionally, this algorithm does not offer a significant advantage in terms of fuel economy.

Table 4 Fuel consumption and travel time under the three driving strategies

Strategy	Fuel consumption (kg)	Travel time (s)
ND	0.49	461
ES-TS	0.43	397
ES-WTS	0.47	292

6 Conclusions

In an urban environment, the majority of fuel consumption in AVs is attributed to frequent acceleration, deceleration, idling, and related factors, accounting for approximately two-thirds of the total fuel consumption. To address this issue, this paper introduces a data-driven rolling eco-speed optimization algorithm designed to smooth vehicle trajectories and decrease fuel consumption. This algorithm combines BP and DBN to utilize traffic state information from both upstream and downstream links, as well as signal phase information from upstream and downstream intersections, to predict short-term traffic conditions. This prediction provides a feasible speed range for subsequent speed optimization, thereby preventing excessive vehicle speeds. The paper also establishes a speed space–time network and presents a rolling eco-speed optimization approach based on the Dijkstra algorithm. Through road tests conducted at four intersections in Shanghai, the proposed algorithm successfully reduces fuel consumption by 12.2% without significant increase in travel time.

Looking ahead, this paper offers several avenues for future expansion and research. The paper can explore the development of a multilayer model to achieve simultaneous optimization of vehicle trajectories and signal phases, potentially leading to further reductions in fuel consumption. It can extend its scope to include multivehicle collaborative trajectory optimization, aiming to minimize unnecessary vehicle braking and enhance overall traffic flow efficiency.

Competing Interests The authors declare that they have no competing interests.

Open Access This article is licensed under a Creative Commons Attribution 4.0 International License, which permits use, sharing, adaptation, distribution and reproduction in any medium or format, as long as you give appropriate credit to the original author(s) and the source, provide a link to the Creative Commons licence, and indicate if changes were made.

The images or other third party material in this article are included in the article's Creative Commons licence, unless indicated otherwise in a credit line to the material. If material is not included in the article's Creative Commons licence and your intended use is not permitted by statutory regulation or exceeds the permitted use, you will need to obtain permission directly from the copyright holder. To view a copy of this licence, visit http://creativecommons.org/licenses/by/4.0/.

References

Ali Y, Zheng Z, Haque M M (2021). Modelling lane-changing execution behaviour in a connected environment: A grouped random parameters with heterogeneity-in-means approach. Communications in Transportation Research, 1: 100009

Almannaa M H, Chen H, Rakha H A, Loulizi A, El-Shawarby I (2019). Field implementation and testing of an automated eco-cooperative adaptive cruise control system in the vicinity of signalized intersections. Transportation Research Part D: Transport and Environment, 67: 244–262

Argonne National Laboratory (2023). Publicly available testing data for advanced technology vehicles

Asadi B, Vahidi A (2011). Predictive cruise control: Utilizing upcoming traffic signal information for improving fuel economy and reducing trip time. IEEE Transactions on Control Systems Technology, 19(3): 707–714

Barth M, Boriboonsomsin K (2009). Energy and emissions impacts of a freeway-based dynamic eco-driving system. Transportation Research Part D: Transport and Environment, 14(6): 400–410

Chen X, Qian L, Wang Q (2022). Eco-driving at signalized intersections under uncertain traffic conditions. Proceedings of the Institution of Mechanical Engineers, Part D: Journal of Automobile Engineering, in press, doi:10.1177/09544070221128181

Cui S H, Cao F, Yu B, Yao B Z (2022a). Modeling heterogeneous traffic mixing regular, connected and connected-autonomous vehicles under connected environment. IEEE Transactions on Intelligent Transportation Systems, 23(7): 8579–8594

Cui S H, Xue Y J, Gao K, Lv M L, Yu B (2023). Adaptive collision-free trajectory tracking control for string stable bidirectional platoons. IEEE Transactions on Intelligent Transportation Systems, 24(11): 12141–12153

Cui S H, Xue Y J, Lv M L, Yao B Z, Yu B (2022b). Cooperative constrained control of autonomous vehicles with nonuniform input quantization. IEEE Transactions on Vehicular Technology, 71(11): 11431–11442

de Nunzio G, de Wit C C, Moulin P, Di Domenico D (2016). Eco-driving in urban traffic networks using traffic signals information. International Journal of Robust and Nonlinear Control, 26(6): 1307–1324

Dong S, Chen H, Gao B, Guo L, Liu Q (2022). Hierarchical energy-efficient control for CAVs at multiple signalized intersections considering queue effects. IEEE Transactions on Intelligent Transportation Systems, 23(8): 11643–11653

Goldmann K, Sieg G (2020). Economic implications of phantom traffic jams: Evidence from traffic experiments. Transportation Letters, 12(6): 386–390

Guo G, Wang Q (2019). Fuel-efficient en route speed planning and tracking control of truck platoons. IEEE Transactions on Intelligent Transportation Systems, 20(8): 3091–3103

Guo X Y, Zhang G, Jia A F (2023). Study on mixed traffic of autonomous vehicles and human-driven vehicles with different cyber interaction approaches. Vehicular Communications, 39: 100550

Hu L, Zhong Y X, Hao W, Moghimi B, Huang J, Zhang X, Du R H (2018). Optimal route algorithm considering traffic light and energy consumption. IEEE Access, 6: 59695–59704

Jafaripournimchahi A, Cai Y F, Wang H, Sun L, Tang Y L, Babadi A A (2023). A viscous continuum traffic flow model based on the cooperative car-following behaviour of connected and autonomous vehicles. IET Intelligent Transport Systems, 17(5): 973–991

Jia L M, Shi R F, Ji L, Wu P (2022). Road transportation and energy integration strategy in China. Strategic Study of CAE, 24(3): 163–172 (in Chinese)

Jiang N, Yu B, Cao F, Dang P F, Cui S H (2021). An extended visual angle car-following model considering the vehicle types in the adjacent lane. Physica A, 566: 125665

Kabir R, Remias S M, Waddell J, Zhu D X (2023). Time-Series fuel consumption prediction assessing delay impacts on energy using vehicular trajectory. Transportation Research Part D: Transport and Environment, 117: 103678

Kamal M A S, Mukai M, Murata J, Kawabe T (2010). Ecological driver assistance system using model-based anticipation of vehicle-road-traffic information. IET Intelligent Transport Systems, 4(4): 244–251

Larsson J, Keskin M F, Peng B, Kulcsár B, Wymeersch H (2021). Prosocial control of connected automated vehicles in mixed-autonomy multi-lane highway traffic. Communications in Transportation Research, 1: 100019

Li M, Wu X K, He X Z, Yu G Z, Wang Y P (2018). An eco-driving system for electric vehicles with signal control under V2X environment. Transportation Research Part C: Emerging Technologies, 93: 335–350

Li T, Gopalswamy S (2021). A spatial searching method for planning under time-dependent constraints for eco-driving in signalized traffic intersection. IEEE Robotics and Automation Letters, 6(2): 2525–2532

Liu B, Sun C, Wang B, Sun F (2022). Adaptive speed planning of connected and automated vehicles using multi-light trained deep reinforcement learning. IEEE Transactions on Vehicular Technology, 71(4): 3533–3546

Liu J, Wang Z, Hou Y, Qu C, Hong J, Lin N (2021). Data-driven energy management and velocity prediction for four-wheel-independent driving electric vehicles. eTransportation, 9: 100119

Liu J Z, Wang Z P, Zhang L (2023). Efficient eco-driving control for EV platoons in mixed urban traffic scenarios considering regenerative braking. IEEE Transactions on Transportation Electrification, in press, doi:10.1109/TTE.2023.3305773

Luo Y, Li S, Zhang S, Qin Z, Li K (2017). Green light optimal speed advisory for hybrid electric vehicles. Mechanical Systems and Signal Processing, 87: 30–44

Ma F W, Yang Y, Wang J W, Li X C, Wu G P, Zhao Y, Wu L, Aksun-Guvenc B, Guvenc L (2021). Eco-driving-based cooperative adaptive cruise control of connected vehicles platoon at signalized intersections. Transportation Research Part D: Transport and Environment, 92: 102746

Munoz-Organero M, Magana V C (2013). Validating the impact on reducing fuel consumption by using an eco-driving assistant based on traffic sign detection and optimal deceleration patterns. IEEE Transactions on Intelligent Transportation Systems, 14(2): 1023–1028

Pi D, Xue P, Xie B, Wang H, Tang X, Hu X (2022). A platoon control method based on DMPC for connected energy-saving electric vehicles. IEEE Transactions on Transportation Electrification, 8(3): 3219–3235

Reza Amini M, Feng Y H, Yang Z, Kolmanovsky I, Sun J (2020). Long-term vehicle speed prediction via historical traffic data analysis for improved energy efficiency of connected electric vehicles. Transportation Research Record: Journal of the Transportation Research Board, 2674(11): 17–29

Shi J, Qiao F, Li Q, Yu L, Hu Y (2018). Application and evaluation of the reinforcement learning approach to eco-driving at intersections under Infrastructure-to-Vehicle communications. Transportation Research Record: Journal of the Transportation Research Board, 2672(25): 89–98

Wang Z, Wu G, Hao P, Boriboonsomsin K, Barth M (2017). Developing a platoon-wide eco-cooperative adaptive cruise control (CACC) system. In: IEEE Intelligent Vehicles Symposium (IV). Los Angeles, CA: IEEE, 1256–1261

Wu C, Zhao G, Ou B (2011). A fuel economy optimization system with applications in vehicles with human drivers and autonomous vehicles. Transportation Research Part D: Transport and Environment, 16(7): 515–524

Wu G, Hao P, Wang Z, Jiang Y, Boriboonsomsin K, Barth M, McConnel M, Qiang S W, Stark J (2021). Eco-approach and departure along signalized corridors considering powertrain characteristics. SAE International Journal of Sustainable Transportation, Energy, Environment, & Policy, 2(1): 25–40

Wu S M, Chen Z, Shen S Q, Shen J W, Guo F X, Liu Y G, Zhang Y J (2023). Hierarchical cooperative eco-driving control for connected autonomous vehicle platoon at signalized intersections. IET Intelligent Transport Systems, 17(8): 1560–1574

Xia H, Boriboonsomsin K, Barth M (2013). Dynamic eco-driving for signalized arterial corridors and its indirect network-wide energy/emissions benefits. Journal of Intelligent Transport Systems, 17(1): 31–41

Yang H, Rakha H, Ala M V (2016). Eco-cooperative adaptive cruise control at signalized intersections considering queue effects. IEEE Transactions on Intelligent Transportation Systems, 18(6): 1575–1585

Yang Z, Feng Y H, Liu H X (2021). A cooperative driving framework for urban arterials in mixed traffic conditions. Transportation Research Part C: Emerging Technologies, 124: 102918

Yu B, Zhou H X, Wang L, Wang Z R, Cui S H (2021). An extended two-lane car-following model considering the influence of heterogeneous speed information on drivers with different characteristics under honk environment. Physica A, 578: 126022

Zhang X, Zhang T, Zou Y, Du G, Guo N (2020). Predictive eco-driving application considering real-world traffic flow. IEEE Access, 8: 82187–82200

Zhang X Z, Fang S C, Shen Y P, Yuan X F, Lu Z Y (2023). Hierarchical velocity optimization for connected automated vehicles with cellular vehicle-to-everything communication at continuous signalized intersections. IEEE Transactions on Intelligent Transportation Systems, in press, doi:10.1109/TITS.2023.3274580

Zhu J, Easa S, Gao K (2022). Merging control strategies of connected and autonomous vehicles at freeway on-ramps: A comprehensive review. Journal of Intelligent and Connected Vehicles, 5(2): 99–111